Journal of Sound and Vibration (2002) **258**(2), 247–268
doi:10.1006/jsvi.5108, available online at http://www.idealibrary.com on IDEAL®

FRICTIONAL BEHAVIOUR OF A BELT-DRIVEN AND PERIODICALLY EXCITED OSCILLATOR

C.-S. Liu and W.-T. Chang

Department of Mechanical and Marine Engineering, National Taiwan Ocean University, 202-24 Keelung, Taiwan, Republic of China. E-mail: csliu@mail.ntou.edu.tw

(*Received* 18 *September* 2001, *and in final form* 11 *January* 2002)

A single-degree-of-freedom system with the parallel presence of a linear spring, a viscous damper and a contact dry friction device is studied here. The mass may slide or stick on the belt when the driver moves periodically or at a constant speed. We derive closed-form solutions according to a more complete two-phase formulation, and some interesting behaviours of the considered system are displayed. For the non-damping oscillator belt with fixed, we offer closed-form formulae for estimating the maximum displacement and the minimum driving speed amplitude needed to prevent sticking. Two friction laws are considered. For the Coulomb friction system, the positive damping term suffices to avoid the climb motion of the mass slider. We also investigate the friction behaviour of the mass slider under the influence of the friction force bound on mass speed, whose curve has negative slope when the mass speed is less than a certain value v_{min}. For the speed-dependent friction system we identify a critical speed denoted by v^*. According to the qualitative analysis in the phase plane we give simple criteria of the parameter values for stable equilibrium point as well as for stable limit cycle. When v varies from $v > v^*$ to $v < v^*$, subcritical Hopf bifurcation occurs. For the latter case the mass slider undergoes a slide–stick motion, but by increasing the driving speed the slide–stick motion can be avoided.

1. INTRODUCTION

In this paper we study a single-degree-of-freedom model with the parallel presence of a linear spring, a linear viscous damper and a dry contact friction between mass slider and running belt. The driver, moving periodically with speed $v\cos\omega_d t$, is connected to the mass slider through a linear spring with stiffness $k > 0$, and a linear viscous damper with no constraint on the viscous coefficient c. The mass is further mounted on a belt which runs forward with a constant speed v_0. A schematic drawing of the mechanical elements' arrangement is shown in Figure 1. It is a belt driven together with a periodically forcing oscillator system.

According to the model described in Figure 1 we can plot the free body diagram as shown in Figure 2, where $m\ddot{x}$ represents the inertial force of the mass slider, $c(\dot{x} - v\cos\omega_d t)$ is the viscous force, $k[x - (v\sin\omega_d t)/\omega_d]$ is the elastic force due to the action of a linear spring, and r_a is the contact friction force. The direction of $m\ddot{x}$ pointing to the left-hand side means that the inertial force is induced by the motion $x(t)$, which points to the right-hand side. Hence, by balancing the inertial force to the other three forces, we obtain the equation of motion of the mass slider as follows:

$$m\ddot{x}(t) + c[\dot{x}(t) - v\cos\omega_d t] + k\left[x(t) - \frac{v}{\omega_d}\sin\omega_d t\right] + r_a(t) = 0. \tag{1}$$

0022-460X/02/$35.00

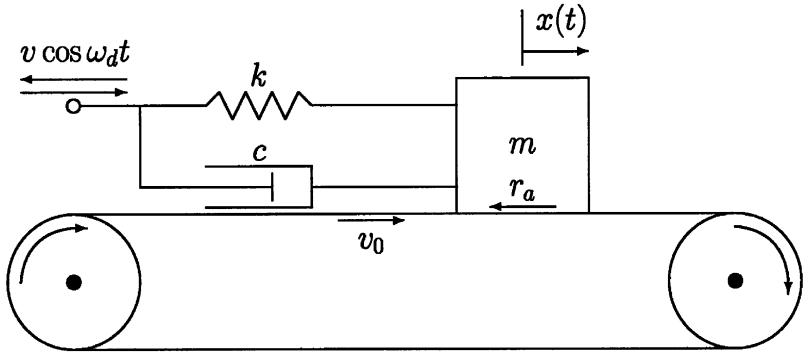

Figure 1. Mass-spring-viscous-friction slider, where friction refers to dry friction between the mass slider and the running belt.

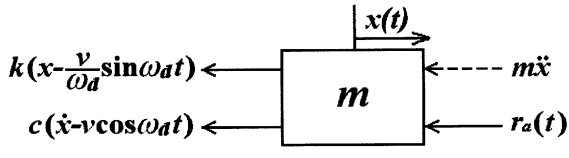

Figure 2. Free body diagram of the system.

TABLE 1

Parameters corresponding to three special cases

	v	ω_d	v_0
Belt-driven system	$v=0$	–	$v_0>0$
Transmission system	$v>0$	$\omega_d=0$	$v_0=0$
Periodically excited system	$v>0$	$\omega_d>0$	$v_0=0$

Let $u(t):=x(t)-v_0t$ denote the relative displacement of the mass slider to the belt; hence, $\dot{u}(t)=\dot{x}(t)-v_0$ and $\ddot{u}(t)=\ddot{x}(t)$ follow, and equation (1) changes to

$$m\ddot{u}(t)+c\dot{u}(t)+ku(t)+r_a(t)=c[v\cos\omega_d t-v_0]+k\left[\frac{v}{\omega_d}\sin\omega_d t-v_0t\right]. \tag{2}$$

Denoting the right side by

$$p(t):=c[v\cos\omega_d t-v_0]+k\left[\frac{v}{\omega_d}\sin\omega_d t-v_0t\right], \tag{3}$$

equation (2) amounts to investigating the displacement $u(t)$ of an oscillator subjected to external force $p(t)$ and friction force $r_a(t)$.

The above system includes three special cases as demonstrated in Table 1. The special case with $v_0=0$ is a periodically excited system, of which equation (2)

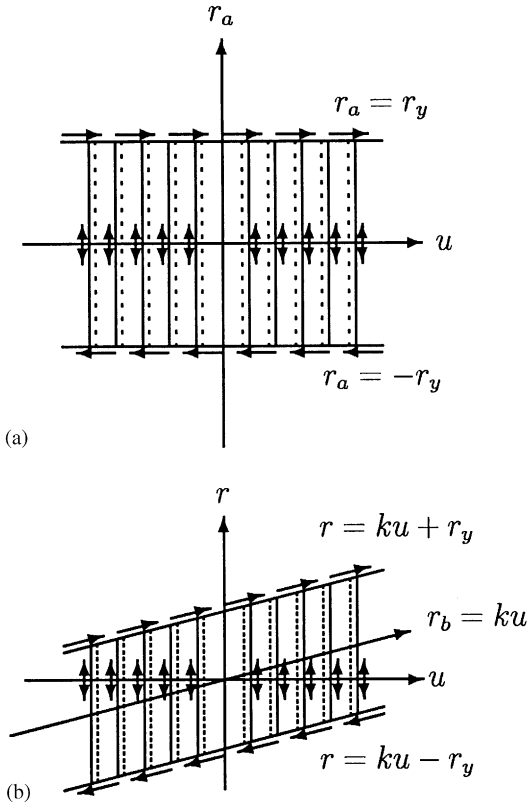

Figure 3. Coulomb friction model: (a) relation of friction force r_a and relative displacement u; (b) relation of restoring force r and relative displacement u.

can be recast to

$$m\frac{\mathrm{d}^2u(\tau)}{\mathrm{d}\tau^2} + c\frac{\mathrm{d}u(\tau)}{\mathrm{d}\tau} + ku(\tau) + r_a(\tau) = v\sqrt{c^2 + \frac{k^2}{\omega_d^2}}\sin\omega_d\tau, \tag{4}$$

where $\tau = t + (1/\omega_d)\arctan(c\omega_d/k)$. The above special case together with the Coulomb friction law for r_a has been investigated by many researchers; see e.g., references [1–5]. The belt-driven system, i.e., $v = 0$ and $v_0 > 0$, together with the Coulomb friction law and a speed-dependent friction law has been employed by Liu [6] to analyze the self-excited problem in metal cutting. Popp *et al.* [7] have investigated a similar system as the one shown in Figure 1 but with $c = 0$, and displayed the dynamic behaviour via three-dimensional phase portraits and the Poincré cross-section method, observing stick–slip chaos. More recently, Andreaus and Casini [8] have investigated a similar moving base together with a periodically exciting system with switch model for friction force, and have shown that the considered system undergoes a periodic-doubling cascade to chaos by increasing the frequency ratio.

In this paper we first give some interesting phenomena of the general system behaviour. A complete formulation of the Coulomb friction law led us easily to calculate the responses according to the two-phase closed-form solutions. Then we consider a more simple arrangement of the system with $\omega_d = 0$ and $v_0 = 0$. But we consider two models of the dry friction: Coulomb friction model (see Figure 3) and a speed-dependent friction

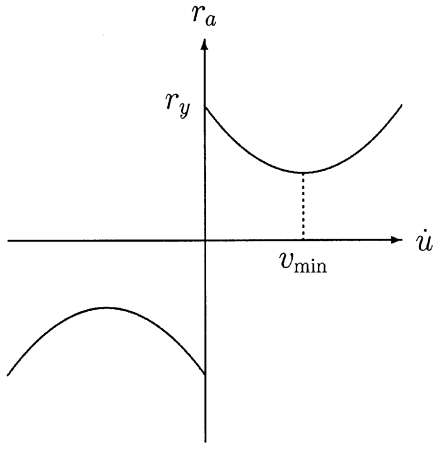

Figure 4. Friction force of the speed-dependent friction model depends on mass velocity through the relation $r_a = r_y \operatorname{sgn}(\dot{u}) - \alpha_1 \dot{u} + \alpha_2 \dot{u}^3$, where α_1 and α_2 are experimentally determined constants.

model (see Figure 4). The first model assumes that the friction law between the mass slider and the belt obeys the relation as shown in Figure 3(a), where r_a denotes the constant friction force and r_y is a constant friction force bound independent of mass relative speed. The resulting system includes five parameters, namely the mass m of the slider, the stiffness k and the viscous coefficient c of support component, the friction force bound r_y between mass slider and belt, and the driver moving speed v. It is a simple model to simulate the self-excited vibration behaviour of mass transmission due to contact friction. Then, in addition to the above five-parameters model the second model also includes another two constants α_1 and α_2, which reflects the non-linear dependence of the friction force bound on mass relative speed.

2. MODELLING COULOMB FRICTION

The conventional two-valuedness representation of the Coulomb's friction law is usually expressed as

$$r_a(t) = \begin{cases} r_y & \text{if } \dot{u} > 0 \text{ or } \dot{x} > v_0, \\ -r_y & \text{if } \dot{u} < 0 \text{ or } \dot{x} < v_0. \end{cases}$$

This formalism is correct but incomplete. In fact, the friction force r_a may take any value between $-r_y$ and r_y when $\dot{u} = 0$; therefore, the following expression provides a more precise description:

$$r_a(t) \begin{cases} = r_y & \text{if } \dot{u} > 0 \text{ or } \dot{x} > v_0, \\ \in [-r_y, r_y] & \text{if } \dot{u} = 0 \text{ or } \dot{x} = v_0, \\ = -r_y & \text{if } \dot{u} < 0 \text{ or } \dot{x} < v_0. \end{cases}$$

Nevertheless, the above formalism, although correct, is not complete yet, since it still lacks a two-way relation between $\dot{u}$ and r_a. For completeness we need a sliding rule and a complementary trio as follows [4]:

$$\dot{u} = \frac{\dot{\Lambda}}{r_y^2} r_a, \quad |r_a| \leqslant r_y, \quad \dot{\Lambda} \geqslant 0, \quad |r_a| \dot{\Lambda} = r_y \dot{\Lambda}, \tag{5-8}$$

where $\dot{\Lambda}$ is the friction power, so that Λ is the dissipated energy due to friction. Equation (5) is a sliding rule, which duplicates a two-way relation between r_a and $\dot{u}$ as shown in Figure 3(a). More importantly, it depicts the relation of r_a to u, not to $\dot{u}$ as the conventional ones are.

The restoring force $r(t)$ of the mass slider can be defined as

$$r = r_a + r_b, \tag{9}$$

with r_a modelled by equations (5)–(8) and r_b by

$$\dot{r}_b = k\dot{u}. \tag{10}$$

Thus, the relation between the restoring force function $r(t)$ and the relative displacement function $u(t)$ is described by equations (5)–(10), which may be schematically illustrated in Figure 3(b).

According to the above descriptions, the mass slider can be either in the sticking phase or in the sliding phase according to the values of $\dot{\Lambda}$ and r_a as follows:

$$\dot{\Lambda} > 0 \text{ and } |r_a| = r_y \;\Rightarrow\; \dot{\Lambda} = r_a\dot{u} > 0 \text{ sliding phase},$$
$$\dot{\Lambda} = 0 \text{ and } |r_a| \leqslant r_y \;\Rightarrow\; \dot{\Lambda} = r_a\dot{u} = 0 \text{ sticking phase}.$$

Phase (i) is nothing but the *sliding phase*, since $\dot{\Lambda} = r_a\dot{u} > 0$ and $\dot{u} \neq 0$, so that the contact surfaces slide relative to each other and dissipation occurs due to friction between the sliding surfaces. Phase (ii) is obviously the *sticking phase*, since $\dot{\Lambda} = 0$ drastically reduces equation (5) to $\dot{u} = 0$, which indicates that the contact surfaces are sticking together. In the sliding phase, the sliding friction causes positive friction dissipation, while in the sticking phase the mass slider sticks on the surface of the belt and no friction dissipation occurs. Thus the history of the motion of the mass slider may be composed of a succession of contiguous time intervals, sliding-phase intervals being interlaced with sticking-phase intervals, but the time duration of a sticking-phase interval can be finite, infinite (permanent sticking) or zero.

3. GOVERNING EQUATIONS

In terms of $r(t)$ equation (2) can be written as

$$m\ddot{u}(t) + c\dot{u}(t) + r(t) = p(t). \tag{11}$$

By considering the initial values of $r(t_i)$, $r_a(t_i)$ and $u(t_i)$ at an initial time t_i, the above $r(t)$, in view of equations (9) and (10), can be re-expressed as

$$r(t) = r(t_i) + r_a(t) - r_a(t_i) + k[u(t) - u(t_i)]. \tag{12}$$

Substituting it into equation (11), we obtain

$$m\ddot{u}(t) + c\dot{u}(t) + ku(t) + r_a(t) = p(t) - r(t_i) + r_a(t_i) + ku(t_i). \tag{13}$$

3.1. SLIDING PHASE

In a sliding-phase interval, $|r_a| = r_y$ and $r_a(t) = r_a(t_i)$, equations (12) and (13) can be reduced, respectively, to

$$r(t) = r(t_i) + k[u(t) - u(t_i)], \tag{14}$$

$$m\ddot{u}(t) + c\dot{u}(t) + ku(t) = p(t) - r(t_i) + ku(t_i), \tag{15}$$

where the initial time t_i is chosen to be the start-to-side time t_{slide} of the sliding-phase interval. Hence, equations (14) and (15) together are the sliding-phase governing equations for $r(t)$ and $u(t)$.

3.2. STICKING PHASE

In a sticking-phase interval, $\dot{\Lambda} = 0$, $\dot{u} = 0$ and $\ddot{u} = 0$, equation (11) simply reduces to

$$r(t) = p(t), \tag{16}$$

and

$$u(t) = u(t_i) \tag{17}$$

follows directly, where the initial time t_i is chosen to be the start-to-stick time t_{stick} of the sticking-phase interval. Equations (16) and (17) together are the sticking-phase governing equations for $r(t)$ and $u(t)$.

3.3. SLIDE–SLIDE CONDITION

It is interesting to find the condition under which the time duration of a sticking-phase interval is zero. The transition (say at time t) from a sliding-phase interval to a sticking-phase interval of non-zero time duration is possible only if $|p(t) - ku(t)| < r_y$. Otherwise, a sliding-phase interval will continue to another sliding-phase interval with a sticking phase of zero time duration present in between the two sliding-phase intervals. The above type of motion may be called the slide–slide motion.

If at the time instant t

$$|p(t) - ku(t)| \geqslant r_y, \tag{18}$$

the duration of the sticking-phase interval is zero, resulting in the mass slider moving from a sliding-phase interval to another sliding-phase interval. Therefore, equation (18) may be called the slide–slide condition. Stops with zero duration may be further classified into two types [3,4]: normal stop and abnormal stop. The former occurs when the relative displacement reaches a local extremum and $\dot{u}(t)$ reverses its sign after a turning point. The criteria for normal stop are

$$|p(t) - ku(t)| \geqslant r_y \quad \text{and} \quad r_a(t)\ddot{u}(t) < 0 \tag{19}$$

at the time moment t with $\dot{u}(t) = 0$. The criteria for abnormal stop are

$$|p(t) - ku(t)| \geqslant r_y \quad \text{and} \quad r_a(t)\ddot{u}(t) > 0 \tag{20}$$

at the time moment t with $\dot{u}(t) = 0$. The latter condition leads to $\dot{u}(t^+) > 0$ if $r_a(t) > 0$ and $\dot{u}(t^+) < 0$ if $r_a(t) < 0$, which indicates that the abnormal stop occurs when the relative displacement reaches a local extremum and, upon separation, $\dot{u}(t)$ does not change its sign as the one prior to the stop has.

4. RESPONSES OF FRICTION OSCILLATOR

In what follows we will derive the exact solutions in the sliding phase and decide the values of t_{stick} and t_{slide}.

4.1. EXACT SOLUTIONS

In the sliding phase $u(t)$ can be obtained by solving equation (15) for the following three different cases:

Case 1. $c^2-4mk>0$ (over-damped $\zeta>1$):

$$u(t) = C_1 \exp[\omega_n(-\zeta + \sqrt{\zeta^2-1})(t-t_i)] + C_2 \exp[\omega_n(-\zeta - \sqrt{\zeta^2-1})(t-t_i)] + D_1 \sin\omega_d t + D_2 \cos\omega_d t - v_0 t + u(t_i) - \frac{r(t_i)}{k}, \tag{21}$$

where

$$\omega_n \coloneqq \sqrt{\frac{k}{m}}, \quad \zeta \coloneqq \frac{c}{2m\omega_n} \tag{22, 23}$$

are, respectively, the natural frequency and damping ratio, and

$$D_1 \coloneqq \frac{v[(4\zeta^2-1)r_w^2+1]}{\omega_d r_w^2[4\zeta^2-2+r_w^2]+\omega_d}, \tag{24}$$

$$D_2 \coloneqq \frac{-2v\zeta r_w^3}{\omega_d r_w^2[4\zeta^2-2+r_w^2]+\omega_d}. \tag{25}$$

Here $r_w \coloneqq \omega_d/\omega_n$ denotes the frequency ratio. The above two integration constants are given, respectively, by

$$C_1 \coloneqq \frac{[D_1\omega_n(-\zeta-\sqrt{\zeta^2-1})+D_2\omega_d]\sin\omega_d t_i + [D_2\omega_n(-\zeta-\sqrt{\zeta^2-1})-D_1\omega_d]\cos\omega_d t_i}{2\omega_n\sqrt{\zeta^2-1}} + \frac{\dot{u}(t_i)+v_0-\omega_n(-\zeta-\sqrt{\zeta^2-1})[r(t_i)/k+v_0 t_i]}{2\omega_n\sqrt{\zeta^2-1}}, \tag{26}$$

$$C_2 \coloneqq \frac{[D_1\omega_d - D_2\omega_n(-\zeta+\sqrt{\zeta^2-1})]\cos\omega_d t_i - [D_1\omega_n(-\zeta+\sqrt{\zeta^2-1})+D_2\omega_d]\sin\omega_d t_i}{2\omega_n\sqrt{\zeta^2-1}} - \frac{\dot{u}(t_i)+v_0-\omega_n(-\zeta+\sqrt{\zeta^2-1})[r(t_i)/k+v_0 t_i]}{2\omega_n\sqrt{\zeta^2-1}}. \tag{27}$$

Case 2. $c^2-4mk=0$ (critically damped $\zeta=1$):

$$u(t) = [C_1 + C_2(t-t_i)]\exp[-\omega_n(t-t_i)] + D_1 \sin\omega_d t + D_2 \cos\omega_d t - v_0 t + u(t_i) - \frac{r(t_i)}{k}, \tag{28}$$

where

$$C_1 := \frac{r(t_i)}{k} + v_0 t_i - D_1 \sin \omega_d t_i - D_2 \cos \omega_d t_i, \tag{29}$$

$$\begin{aligned} C_2 := {} & (D_2\omega_d - D_1\omega_n)\sin \omega_d t_i - (D_2\omega_n + D_1\omega_d)\cos \omega_d t_i \\ & + \dot{u}(t_i) + v_0 + \omega_n \left[\frac{r(t_i)}{k} + v_0 t_i \right]. \end{aligned} \tag{30}$$

Case 3. $c^2 - 4mk < 0$ (under-damped $\zeta < 1$):

$$\begin{aligned} u(t) = {} & \exp[-\zeta\omega_n(t - t_i)][C_1 \cos \omega(t - t_i) + C_2 \sin \omega(t - t_i)] \\ & + D_1 \sin \omega_d t + D_2 \cos \omega_d t - v_0 t + u(t_i) - \frac{r(t_i)}{k}, \end{aligned} \tag{31}$$

where

$$\omega := \omega_n \sqrt{1 - \zeta^2} \tag{32}$$

is the damped frequency, and

$$C_1 := \frac{r(t_i)}{k} + v_0 t_i - D_1 \sin \omega_d t_i - D_2 \cos \omega_d t_i, \tag{33}$$

$$\begin{aligned} C_2 := {} & \frac{(D_2\omega_d - D_1\zeta\omega_n)\sin \omega_d t_i - (D_2\zeta\omega_d + D_1\omega_d)\cos \omega_d t_i}{\omega} \\ & + \frac{\dot{u}(t_i) + v_0 + \zeta\omega_n[r(t_i)/k + v_0 t_i]}{\omega}. \end{aligned} \tag{34}$$

4.2. START-TO-SLIDE TIME

The start-to-slide time $t = t_{slide}$, which is the end time of the preceding sticking-phase interval, can be determined by solving

$$\left| k\left(\frac{v}{\omega_d} \sin \omega_d t - v_0 t \right) + c(v \cos \omega_d t - v_0) - ku(t_i) \right| = r_y. \tag{35}$$

However, it needs a numerical method to solve the above equation for t_{slide}.

4.3. START-TO-STICK TIME

The start-to-stick time t_{stick} of the sticking-phase interval is the end time of the preceding sliding-phase interval, which is determined by solving $\dot{u}(t) = 0$ with $u(t)$ given, respectively, by equations (21), (28) and (31) for the three different cases. Because these equations are transcendental in nature we appeal to a numerical scheme to solve them.

4.4. RESPONSES FOR SOME GENERAL CASES

In order to display the different behaviour of the considered friction system, we use the above solutions to calculate the responses as shown in Figure 5 for three different parameter values. For each case we have fixed the same values of $m = 8\,\text{kN s}^2/\text{cm}$ $(= 8 \times 10^5/9{\cdot}81\,\text{kg})$, $\zeta = 0{\cdot}02$, $r_y = 10\,\text{kN}$ and $\omega_d = 2\pi\,\text{rad/s}$. In Figures 5(a)–(e), $r_w = 0{\cdot}5$, $v = 5\,\text{cm/s}$, $v_0 = 1\,\text{cm/s}$ are adopted, and the other parameter values are calculated,

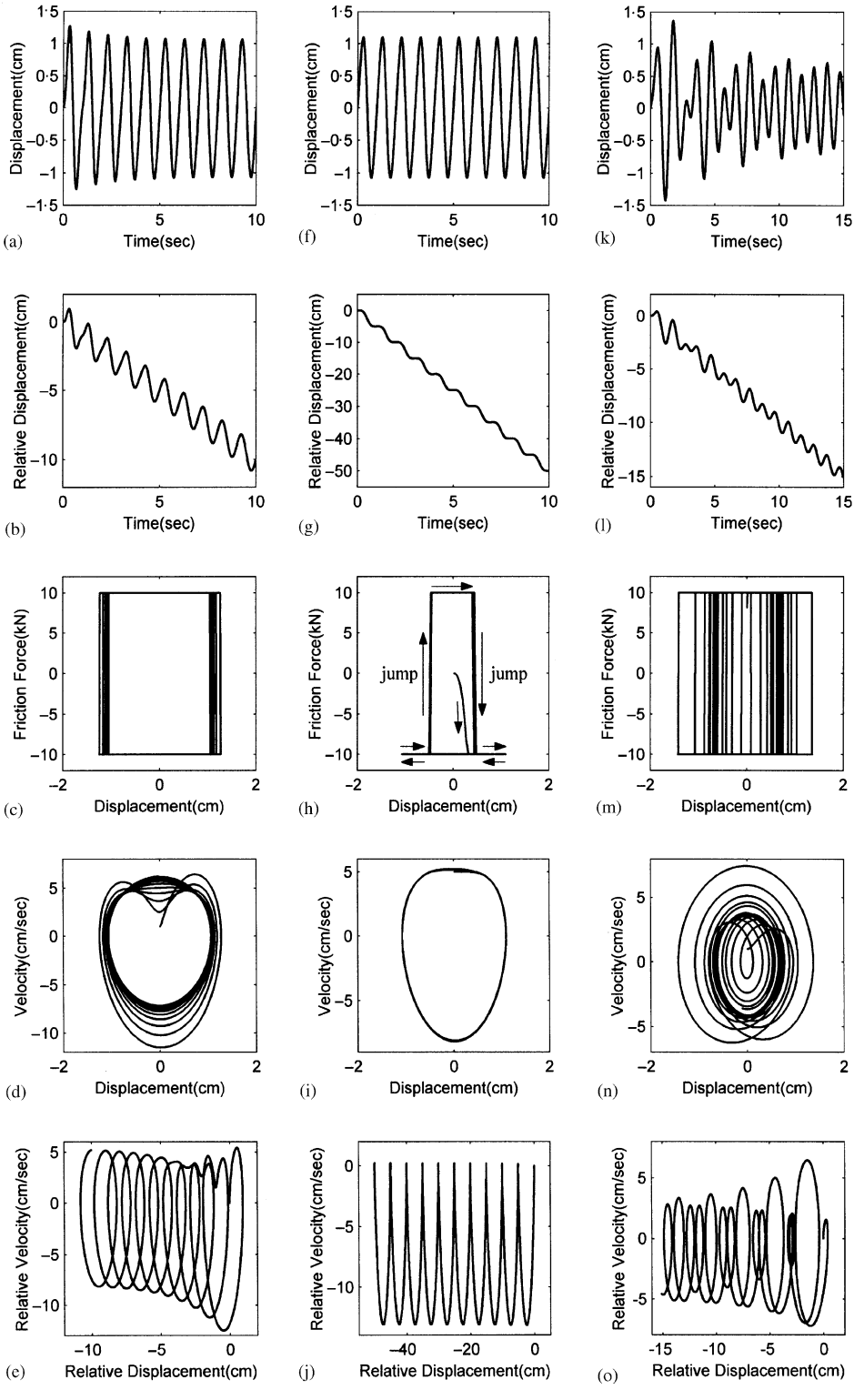

Figure 5. Three typical friction responses of a belt-driven and periodically excited system.

respectively, by $\omega_n = \omega_d / r_w = 4\pi$ rad/s, $k = m\omega_n^2 = 128\pi^2$ kN/cm and $c = 2m\omega_n\zeta = 1{\cdot}28\pi$ kN s/cm. In Figures 5(f)–(j), $r_w = 0{\cdot}5$, $v = v_0 = 5$ cm/s are adopted, and the other parameter values are the same as above. In Figures 5(k)–(o), $r_w = 1{\cdot}5$, $v = 5$ cm/s, $v_0 = 1$ cm/s are adopted, and the other parameter values are $\omega_n = \omega_d / r_w = 4\pi/3$ rad/s, $k = m\omega_n^2 = 128\pi^2/9$ kN/cm and $c = 2m\omega_n\zeta = 1{\cdot}28\pi/3$ kN s/cm. In addition to the initial sticking the motions are all of the slide–slide types. It can be seen that all phase portraits exhibit stabilized limit cycles. However, their sizes are very different. Especially the size of the limit cycle in Figure 5(n) is far less than that in Figures 5(d) and 5(i). The above two limit cycles almost have the same size. It appears that the belt running speed v_0 has little influence on the size of the limit cycle. However, the frequency ratio r_w is an important factor to decide what the size of the limit cycle should be.

5. STEADY STATE RESPONSE FOR THE CASE $v_0 = 0$ AND $c = 0$

For estimating the steady state responses of the system behaviour and investigating the influence of the system parameters, we may employ the phase plane method in our system as that done in reference [5] for a simpler system to derive formulas, which can be used to calculate the maximum displacement and the minimum load amplitude to prevent sticking. For this purpose let us return to equation (1) and consider a simpler case with $c = 0$ and $v_0 = 0$. For such a system, the maximum displacement in the steady state is given by

$$\frac{x_{max}}{x_y} = \sqrt{\left(\frac{m\omega_n v}{r_y r_w (1 - r_w^2)}\right)^2 - \frac{(\sin(\pi/r_w))^2}{r_w^2 (1 + \cos(\pi/r_w))^2}}, \tag{36}$$

where $x_y := r_y/k$. In Figure 6(a) the results calculated by the above formula for several values of $v = 5$, 10, 15, 20, 25 cm/s are displayed. Here we fixed the values with $m = 8$ kN s^2/cm ($= 8 \times 10^5/9{\cdot}81$ kg), $r_y = 10$ kN, $k = 32$ kN/cm, and hence $\omega_n = 2$ rad/s. More importantly, a precise formula for estimating the border line of the domain of steady state slide–slide oscillatory responses in the plane (r_w, v) can be derived as follows:

$$v = \frac{r_w r_y}{m\omega_n} \sqrt{\left(\frac{1}{r_w^2} - 1\right)^2 \left[1 + \left(\frac{r_w \sin(\pi/r_w)}{1 + \cos(\pi/r_w)}\right)^2\right]}. \tag{37}$$

The value of v which is greater than what the above formula predicts will make the oscillator vibratory without stops in the steady state, so that the criterion for zero stop per cycle is

$$v \geqslant \frac{r_w r_y}{m\omega_n} \sqrt{\left(\frac{1}{r_w^2} - 1\right)^2 \left[1 + \left(\frac{r_w \sin(\pi/r_w)}{1 + \cos(\pi/r_w)}\right)^2\right]}. \tag{38}$$

In Figure 6(b) the result calculated by the above formula is displayed. The region of slide–slide motion is marked in the plane (r_w, v).

In steady state estimation for both the belt-driven and periodically excited system however requires a deeper study and will be presented in another place.

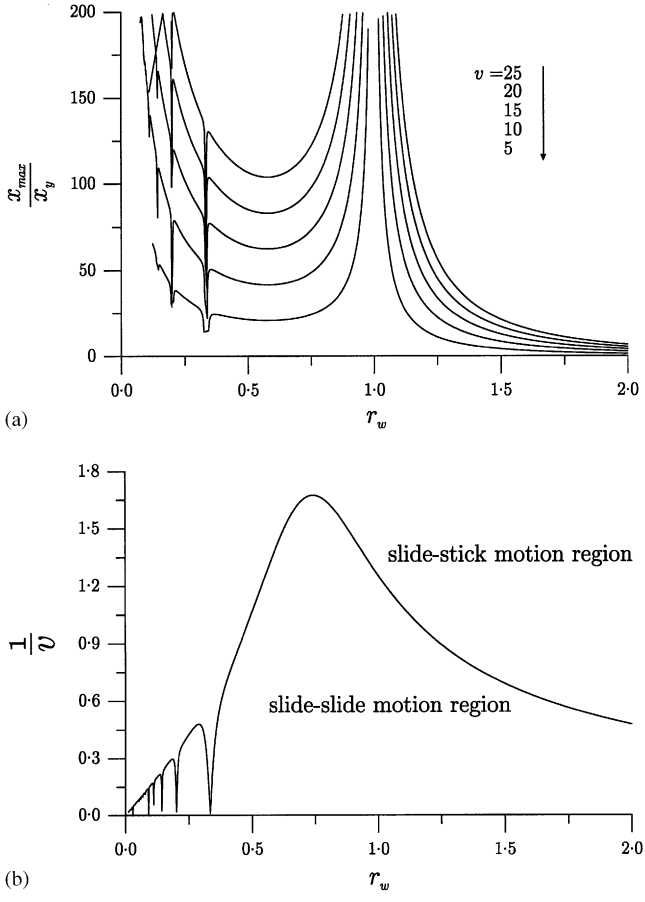

Figure 6. (a) Maximum displacement curves of the system with $c=0$ and $v_0=0$ for several values of v. (b) Minimum driving speed amplitude to prevent sticking.

6. SPECIAL CASE WITH $\omega_d = 0$ AND $v_0 = 0$

Here and henceforth we focus on the special case $\omega_d = 0$ and $v_0=0$, of which $u(t)=x(t)$ and $p(t)=kvt+cv$, and equation (1) reduces to

$$m\ddot{x}(t) + c[\dot{x}(t) - v] + k[x(t) - vt] + r_a(t) = 0. \tag{39}$$

By noting that

$$\lim_{\omega_d \to 0} D_1 \sin \omega_d t = vt,$$

$$\lim_{\omega_d \to 0} D_1 \omega_d \cos \omega_d t = v,$$

$$\lim_{\omega_d \to 0} D_2 \cos \omega_d t = 0,$$

$$\lim_{\omega_d \to 0} D_2 \omega_d \sin \omega_d t = 0,$$

and by using equations (21), (28) and (31) for three different cases, the exact solutions of $x(t)$ in the sliding phase can be derived as follows:

Case 1. $c^2-4mk>0$:

$$x(t) = C_1 \exp[\omega_n(-\zeta + \sqrt{\zeta^2-1})(t-t_i)] + C_2 \exp[\omega_n(-\zeta - \sqrt{\zeta^2-1})(t-t_i)] + vt + x(t_i) - \frac{r(t_i)}{k}, \tag{40}$$

where

$$C_1 := \frac{\dot{x}(t_i) - v - \omega_n(-\zeta - \sqrt{\zeta^2-1})[r(t_i)/k - v_0 t_i]}{2\omega_n\sqrt{\zeta^2-1}}, \tag{41}$$

$$C_2 := \frac{v - \dot{x}(t_i) + \omega_n(-\zeta - \sqrt{\zeta^2-1})[r(t_i)/k - v_0 t_i]}{2\omega_n\sqrt{\zeta^2-1}} + \frac{r(t_i)}{k} - vt_i. \tag{42}$$

Case 2. $c^2-4mk=0$:

$$x(t) = [C_1 + C_2(t-t_i)]\exp[-\omega_n(t-t_i)] + vt + x(t_i) - \frac{r(t_i)}{k}, \tag{43}$$

where

$$C_1 := \frac{r(t_i)}{k} - vt_i, \tag{44}$$

$$C_2 := \dot{x}(t_i) - v + \omega_n\left[\frac{r(t_i)}{k} - vt_i.\right] \tag{45}$$

Case 3. $c^2-4mk<0$:

$$x(t) = \exp[-\zeta\omega_n(t-t_i)][C_1\cos\omega(t-t_i) + C_2\sin\omega(t-t_i)] + vt + x(t_i) - \frac{r(t_i)}{k}, \tag{46}$$

where

$$C_1 := \frac{r(t_i)}{k} - vt_i, \tag{47}$$

$$C_2 := \frac{\dot{x}(t_i) - v + \zeta\omega_n[r(t_i)/k - vt_i]}{\omega}. \tag{48}$$

Owing to the simplicity of the sticking-phase equations, the start-to-slide time $t = t_{slide}$ can be determined exactly by solving

$$|kvt + cv - r_b(t_i)| = r_y. \tag{49}$$

The resultant is

$$t_{slide} = \frac{r_y + kx(t_i) - cv}{kv}. \tag{50}$$

However, if the numerator $r_y + kx(t_i) - cv < 0$ we let $t_{slide} = t_i$.

The start-to-stick time t_{stick} is determined by solving $\dot{x}(t) = 0$ with $x(t)$ given, respectively, by equations (40), (43) and (46) for the three different cases. Because these equations are transcendental in nature, we appeal to the numerical scheme to solve them.

Let $z(t) := x(t) - vt$ denote the relative displacement between mass slider and driver, and $\dot{z}(t) = \dot{x}(t) - v$ and $\ddot{z}(t) = \ddot{x}(t)$ follow; hence, equation (39) can be written as

$$m\ddot{z}(t) + c\dot{z}(t) + kz(t) + r_a(t) = 0, \tag{51}$$

where $r_a(t) = \pm r_y$ in the sliding phase. This equation is rather simple, and as usual we have an unstable focus in the plane $(z, \dot{z})$ for the cases of $c < 0$, stable focus for the cases of $c > 0$, and a centre for the case $c = 0$. We only show results for the last in Figure 7 with $m = 8\,\text{kN s}^2/\text{cm}$ $(= 8 \times 10^5/9{\cdot}81\,\text{kg})$, $k = 32\,\text{kN/cm}$, $r_y = 10\,\text{kN}$ and $v = 5\,\text{cm/s}$. From Figure 7 we can find that when the damping ratio is zero, i.e., $c = 0$, there exist no energy-damped mechanisms in equations (39) and (51), and hence the velocity of the mass slider $\dot{x}$, the relative motion of z, and its velocity $\dot{z}$ all exhibit periodically oscillatory behaviour. Consequently, in the phase plane $(z, \dot{z})$ there is a circle around the equilibrium point $(-0{\cdot}3125, 0)$. Practically, the relative motion between mass slider and driver may cause climb motion, which in turn destroys the uniformity of transmission. For this case it can be seen that upon starting to slide, the mass never comes to stick on the belt. When $\dot{x}$ decreases to zero, the mass immediately undergoes another sliding motion as shown in Figure 7(b), the slide–slide motion, and such type of motion has been named abnormal stop [3, 4], which is due to the single-direction action of the external force.

7. FRICTION FORCE DEPENDING ON MASS SPEED

Instead of the constant friction force bound used in the Coulomb friction model, let us consider a more complicated law of friction force [9]:

$$r_a(t) = r_y \operatorname{sgn}(\dot{x}) - \alpha_1 \dot{x} + \alpha_2 \dot{x}^3, \tag{52}$$

where sgn is the signum function, i.e., $\operatorname{sgn}(\dot{x}) = \dot{x}/|\dot{x}|$ if $\dot{x} \neq 0$, and r_y, α_1 and α_2 are three experimentally determined constants. In Figure 4 the shape of this curve is plotted, where v_{min} denotes the speed value at which the magnitude of friction force is minimum. It shows that the friction force–speed curve may have negative slope when the mass speed is less than the critical value $v_{min} = \sqrt{\alpha_1/(3\alpha_2)}$. It is known that the negative slope is responsible for the energy that is transferred to the vibration, and thus may render self-excited vibration in the course of contact friction [10].

Substituting equation (52) for r_a into equation (39), we obtain

$$m\ddot{x}(t) + c[\dot{x}(t) - v] + k[x(t) - vt] + r_y \operatorname{sgn}(\dot{x}) - \alpha_1 \dot{x}(t) + \alpha_2 \dot{x}^3(t) = 0. \tag{53}$$

As before we let the restoring force be

$$r(t) = r_a(t) + r_b(t) = r_y \operatorname{sgn}(\dot{x}) - \alpha_1 \dot{x}(t) + \alpha_2 \dot{x}^3(t) + kx(t), \tag{54}$$

where

$$r_a(t) \begin{cases} = r_y - \alpha_1 \dot{x} + \alpha_2 \dot{x}^3 & \text{if } \dot{x} > 0 \text{ or } \dot{z} > -v, \\ \in [-r_y, r_y] & \text{if } \dot{x} = 0 \text{ or } \dot{z} = -v, \\ = -r_y - \alpha_1 \dot{x} + \alpha_2 \dot{x}^3 & \text{if } \dot{x} < 0 \text{ or } \dot{z} < -v. \end{cases} \tag{55-57}$$

When $\dot{x} = 0$ the friction force may be any value between $-r_y$ and r_y needing to balance with other forces. In terms of $r(t)$, equation (53) can be written as

$$m\ddot{x}(t) + c\dot{x}(t) + r(t) = p(t), \quad p(t) := kvt + cv, \tag{58, 59}$$

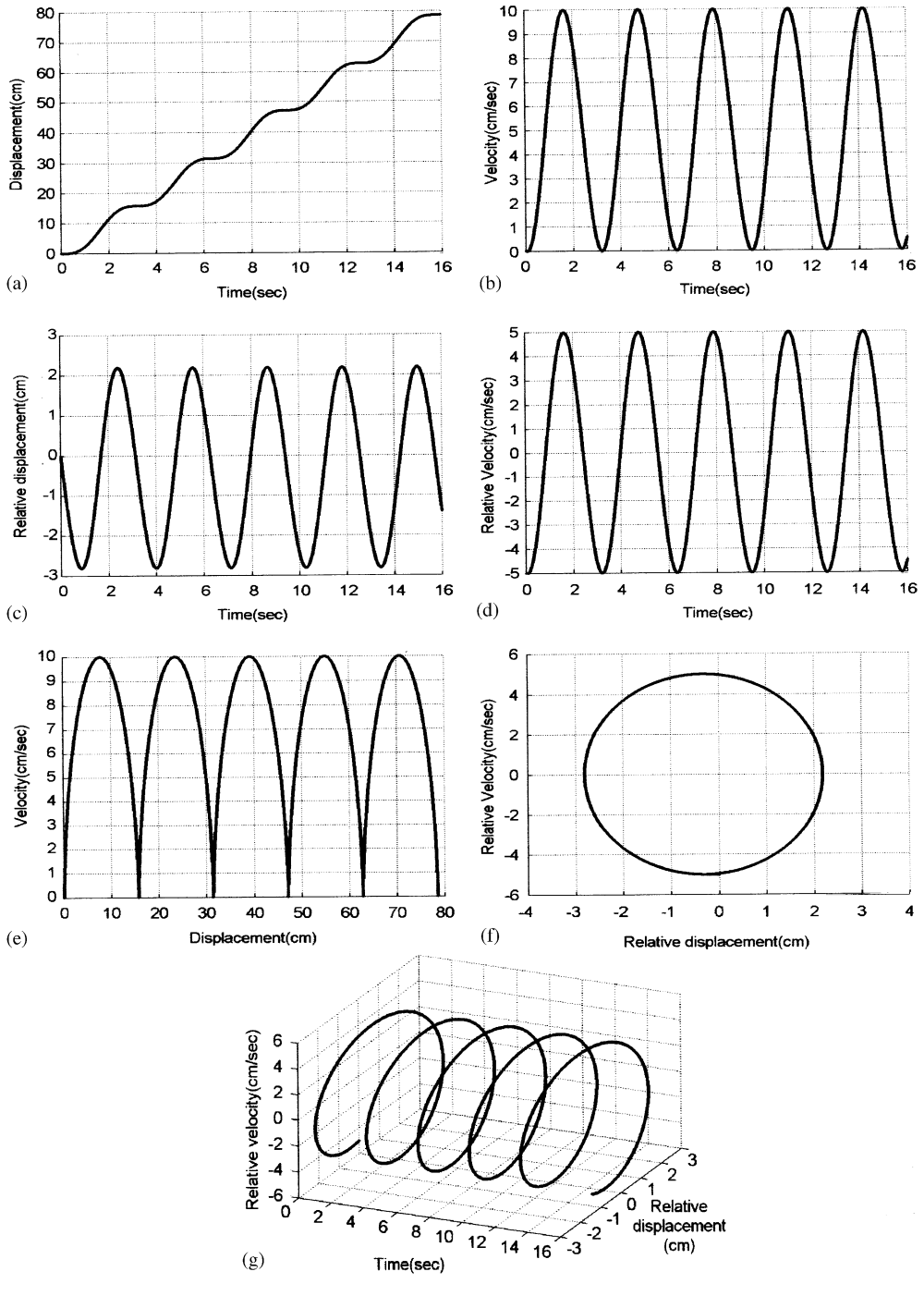

Figure 7. Time history plots and phase plots of the Coulomb friction system with $\zeta = 0$.

where by considering the initial conditions we let

$$r(t) = r(t_i) + r_a(t) - r_a(t_i) + k[x(t) - x(t_i)]. \tag{60}$$

Thus, we get

$$m\ddot{x}(t) + c\dot{x}(t) + kx(t) + r_a(t) = p(t) - r(t_i) + r_a(t_i) + kx(t_i). \tag{61}$$

In a sliding-phase interval, $|\dot{x}(t)| > 0$ and $r_a(t) = r_y \operatorname{sgn}(\dot{x}) - \alpha_1\dot{x}(t) + \alpha_2\dot{x}^3(t)$, equations (61) and (60) can be reduced, respectively, to

$$m\ddot{x}(t) + c\dot{x}(t) + kx(t) - \alpha_1\dot{x}(t) + \alpha_2\dot{x}^3(t) = p(t) - r(t_i) + kx(t_i), \tag{62}$$

$$r(t) = r(t_i) + k[x(t) - x(t_i)] - \alpha_1\dot{x}(t) + \alpha_2\dot{x}^3(t), \tag{63}$$

where the initial time t_i is chosen to be the start-to-slide time t_{slide} of the sliding-phase interval. Hence, equations (62) and (63) together are the sliding-phase governing equations for $x(t)$ and $r(t)$.

In a sticking-phase interval, $\dot{x} = 0$ and $\ddot{x} = 0$, so that $r(t) = p(t)$ and $x(t) = x(t_i)$, where the initial time t_i is chosen to be the start-to-stick time t_{stick} of the sticking-phase interval.

8. QUALITATIVE ANALYSIS OF SYSTEM BEHAVIOUR

If we replace $x(t) - v(t)$ by $z(t)$, $\dot{x}(t) - v$ by $\dot{z}(t)$ and $\ddot{x}(t)$ by $\ddot{z}(t)$, equation (53) can be written as

$$m\ddot{z}(t) + c\dot{z}(t) + kz(t) + r_y \operatorname{sgn}[\dot{z}(t) + v] - \alpha_1[\dot{z}(t) + v] + \alpha_2[\dot{z}(t) + v]^3 = 0. \tag{64}$$

Let $w := \dot{z}$, and the above equation can be written as

$$\frac{\mathrm{d}}{\mathrm{d}t}\begin{bmatrix} z \\ w \end{bmatrix} = \begin{bmatrix} w \\ \frac{1}{m}(\alpha_1(w+v) - \alpha_2(w+v)^3 - r_y \operatorname{sgn}(w+v) - cw - kz) \end{bmatrix} := \begin{bmatrix} f(z,w) \\ g(z,w) \end{bmatrix}. \tag{65}$$

Let $f(z, w) = 0$ and $g(z, w) = 0$. We obtain the equilibrium point

$$(z_0, w_0) = \left(\frac{\alpha_1 v - \alpha_2 v^3 - r_y}{k}, 0\right). \tag{66}$$

Substituting it into the Jacobian matrix for $f(z, w)$ and $g(z, w)$, we get

$$\mathbf{J} = \begin{bmatrix} 0 & 1 \\ -\omega_n^2 & \frac{1}{m}(\alpha_1 - 3\alpha_2 v^2 - c) \end{bmatrix}. \tag{67}$$

The eigenvalues of $\mathbf{J}$ determine the stability of the equilibrium point (z_0, w_0). The characteristic equation for the eigenvalues is

$$\lambda^2 - \operatorname{tr}\mathbf{J}\lambda + \det\mathbf{J} = 0, \tag{68}$$

where

$$\operatorname{tr}\mathbf{J} = \frac{\alpha_1 - 3\alpha_2 v^2 - c}{m}, \quad \det\mathbf{J} = \omega_n^2. \tag{69, 70}$$

Hence the discriminant of equation (68) is given by

$$\Delta = \left(\frac{\alpha_1 - 3\alpha_2 v^2 - c}{m}\right)^2 - 4\omega_n^2. \tag{71}$$

In order to decide the stability type of the equilibrium point, we should consider seven cases as shown in Figure 8. We note that $\det\mathbf{J} = \omega_n^2 > 0$, and for the case $\Delta > 0$ we have either $\operatorname{tr}\mathbf{J} < 0$ or $\operatorname{tr}\mathbf{J} > 0$. For the first case the equilibrium point is a stable node; for the second case the equilibrium point is an unstable node, and the system exhibits limit cycle

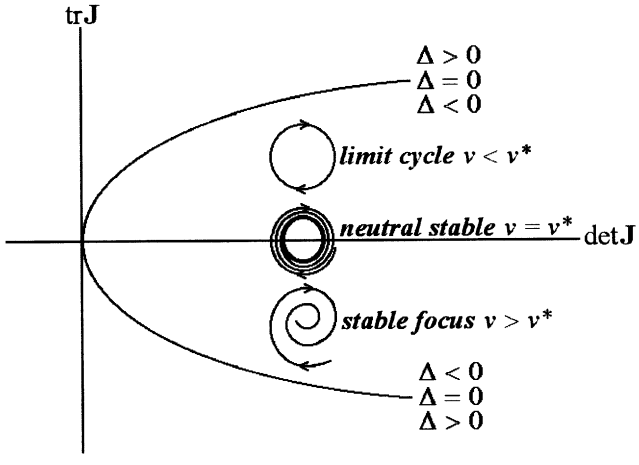

Figure 8. Relations among parameters and stability types of the speed-dependent friction system.

behaviour. For the case $\Delta = 0$ we have either $\mathrm{tr}\,\mathbf{J} < 0$ or $\mathrm{tr}\,\mathbf{J} > 0$. For the first case the equilibrium point is a stable sink; for the second case the equilibrium point is an unstable source, and the system exhibits limit cycle behaviour. For the case $\Delta < 0$, the stability of the equilibrium point is further determined by the values of $\mathrm{tr}\,\mathbf{J}$ as follows:

$$\mathrm{tr}\,\mathbf{J} > 0 \;\Rightarrow\; \alpha_1 - 3\alpha_2 v^2 - c > 0 \;\Rightarrow\; c < \alpha_1 - 3\alpha_2 v^2 \;\Rightarrow\; \text{limit cycle}, \tag{72}$$

$$\mathrm{tr}\,\mathbf{J} = 0 \;\Rightarrow\; \alpha_1 - 3\alpha_2 v^2 - c = 0 \;\Rightarrow\; c = \alpha_1 - 3\alpha_2 v^2 \;\Rightarrow\; \text{neutral centre}, \tag{73}$$

$$\mathrm{tr}\,\mathbf{J} < 0 \;\Rightarrow\; \alpha_1 - 3\alpha_2 v^2 - c < 0 \;\Rightarrow\; c > \alpha_1 - 3\alpha_2 v^2 \;\Rightarrow\; \text{stable focus}. \tag{74}$$

From equations (71) and (72)–(74) we can detect the stability property of the equilibrium point for different parameter values as plotted in Figure 8.

In order to obtain a stable limit cycle, a simple criterion is given as follows:

$$\mathrm{tr}\,\mathbf{J} = \frac{\alpha_1 - 3\alpha_2 v^3 - c}{m} \geqslant 0. \tag{75}$$

Let us denote the critical speed of the driver by

$$v^* := \sqrt{\frac{\alpha_1 - c}{3\alpha_2}}, \tag{76}$$

which slightly deviates from the minimum speed v_{min} for the minimum friction force bound due to the damping constant c. It indicates that when $v > v^*$ ($\mathrm{tr}\,\mathbf{J} < 0$) the mass slider motion tends to a stable equilibrium point, and when $v < v^*$ ($\mathrm{tr}\,\mathbf{J} < 0$) the mass slider motion tends to a stable limit cycle. Thus, we say that when v varies from $v > v^*$ to $v < v^*$ subcritical Hopf bifurcation occurs [11, 12].

On the other hand, solving $\Delta = 0$ we obtain the other two critical speeds:

$$v_1^{**} := \sqrt{\frac{\alpha_1 - c + 2\sqrt{mk}}{3\alpha_2}}, \tag{77}$$

$$v_2^{**} := \sqrt{\frac{\alpha_1 - c - 2\sqrt{mk}}{3\alpha_2}}. \tag{78}$$

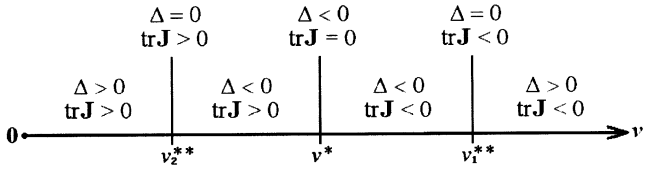

Figure 9. Relations of driving speed v and the values of Δ and $\mathrm{tr}\,\mathbf{J}$ of the speed-dependent friction system.

Obviously, $v_2^{**} < v^* < v_1^{**}$. In Figure 9 we show the relations of Δ, $\mathrm{tr}\,\mathbf{J}$, v_2^{**}, v^* and v_1^{**} in the co-ordinate v. Accordingly, we have the following system behaviour:

$$v_1^{**} < v \;\Rightarrow\; \text{stable node}, \tag{79}$$

$$v = v_1^{**} \;\Rightarrow\; \text{stable infected node}, \tag{80}$$

$$v^* < v < v_1^{**} \;\Rightarrow\; \text{stable focus}, \tag{81}$$

$$v = v^* \;\Rightarrow\; \text{neutral stable centre}, \tag{82}$$

$$v_2^{**} < v < v^* \;\Rightarrow\; \text{limit cycle}, \tag{83}$$

$$v = v_2^{**} \;\Rightarrow\; \text{limit cycle}, \tag{84}$$

$$0 < v < v_2^{**} \;\Rightarrow\; \text{limit cycle}. \tag{85}$$

9. RESPONSES OF SPEED-DEPENDENT FRICTION SYSTEM

By employing the group-preserving scheme [13] we have calculated four types of responses. Some results are shown in Figures 10 and 11 for different $v = 65$, 20, 5, 1·5 cm/s, but the same other parameter values with $m = 8\,\mathrm{kN\,s^2/cm}$ $(= 8 \times 10^5/9{\cdot}81\,\mathrm{kg})$, $k = 32\,\mathrm{kN/cm}$, $c = 0{\cdot}64\,\mathrm{kN\,s/cm}$, $r_y = 10\,\mathrm{kN}$, $\alpha_1 = 1\,\mathrm{kN\,s/cm}$ and $\alpha_2 = 0{\cdot}0048\,\mathrm{kN\,s^3/cm^2}$. For these parameter values we have $v^* = 5\,\mathrm{cm/s}$ and $v_1^{**} = \sqrt{20225/9} \approx 47{\cdot}4\,\mathrm{cm/s}$ and the stability properties of the equilibrium point are summarized as follows:

$$\begin{aligned}
&v = 65 \;\Rightarrow\; v > v_1^{**} \text{ and } v > v^* \;\Rightarrow\; \text{stable node},\\
&v = 20 \;\Rightarrow\; v < v_1^{**} \text{ and } v > v^* \;\Rightarrow\; \text{stable focus},\\
&v = 5 \;\Rightarrow\; v < v_1^{**} \text{ and } v = v^* \;\Rightarrow\; \text{neutral stable centre},\\
&v = 1{\cdot}5 \;\Rightarrow\; v < v_1^{**} \text{ and } v < v^* \;\Rightarrow\; \text{limit cycle}.
\end{aligned}$$

When the driving velocity is $v = 65\,\mathrm{cm/s}$, the speed-dependent friction system behaves like an over-damped system, and the input energy is damped out very quickly. For this case the velocity of the mass slider $\dot{x}$ quickly approaches the value of the driver $v = 65\,\mathrm{cm/s}$, and the relative displacement z and its velocity $\dot{z}$ tend to the stable node point $(z, \dot{z}) = (-39{\cdot}475, 0)$ very soon as shown in Figure 10(a). From Figure 10(b) we can find that when the driving velocity is $v = 20\,\mathrm{cm/s}$, the equilibrium point is of stable focus type, and the system behaves like an under-damped system. The oscillating amplitudes of the velocity $\dot{x}$, of the relative displacement z and of its velocity $\dot{z}$ are all decreased. In the phase plane $(z, \dot{z})$, the trajectory is spiraled gradually into the focus point $(-0{\cdot}8875, 0)$, and the relative

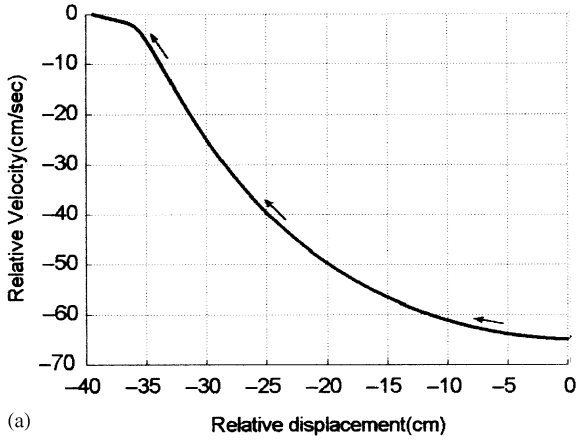

(a)

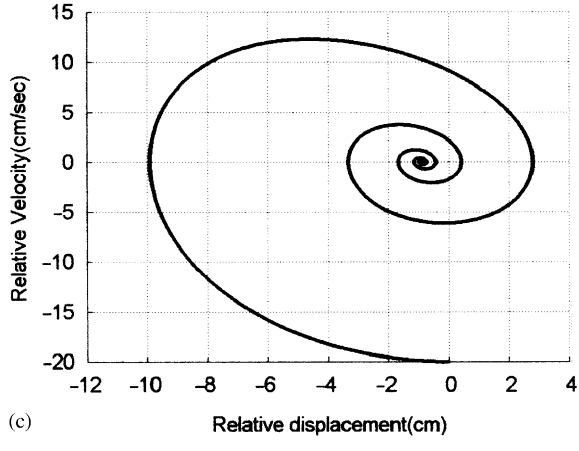

(c)

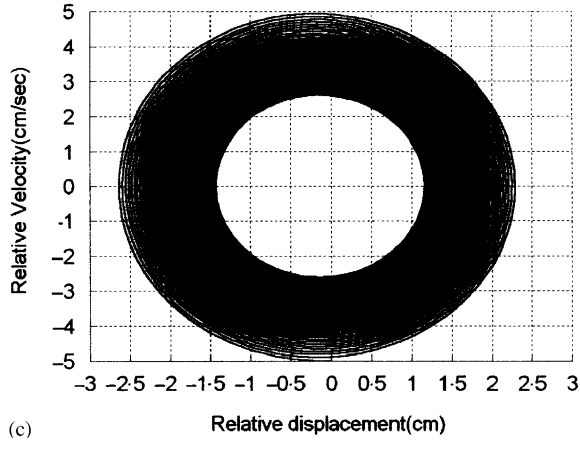

(c)

Figure 10. Phase plots of the speed-dependent friction system with (a) $v = 65\,\text{cm/s}$, (b) $v = 20\,\text{cm/s}$ and (c) $v = 5\,\text{cm/s}$.

motion between the mass slider and the driver converges to a constant value. When the driving velocity is $v = 5\,\text{cm/s}$, the equilibrium point is of neutral stable centre type, and the system still behaves like a slightly under-damped system in the first few hundred seconds.

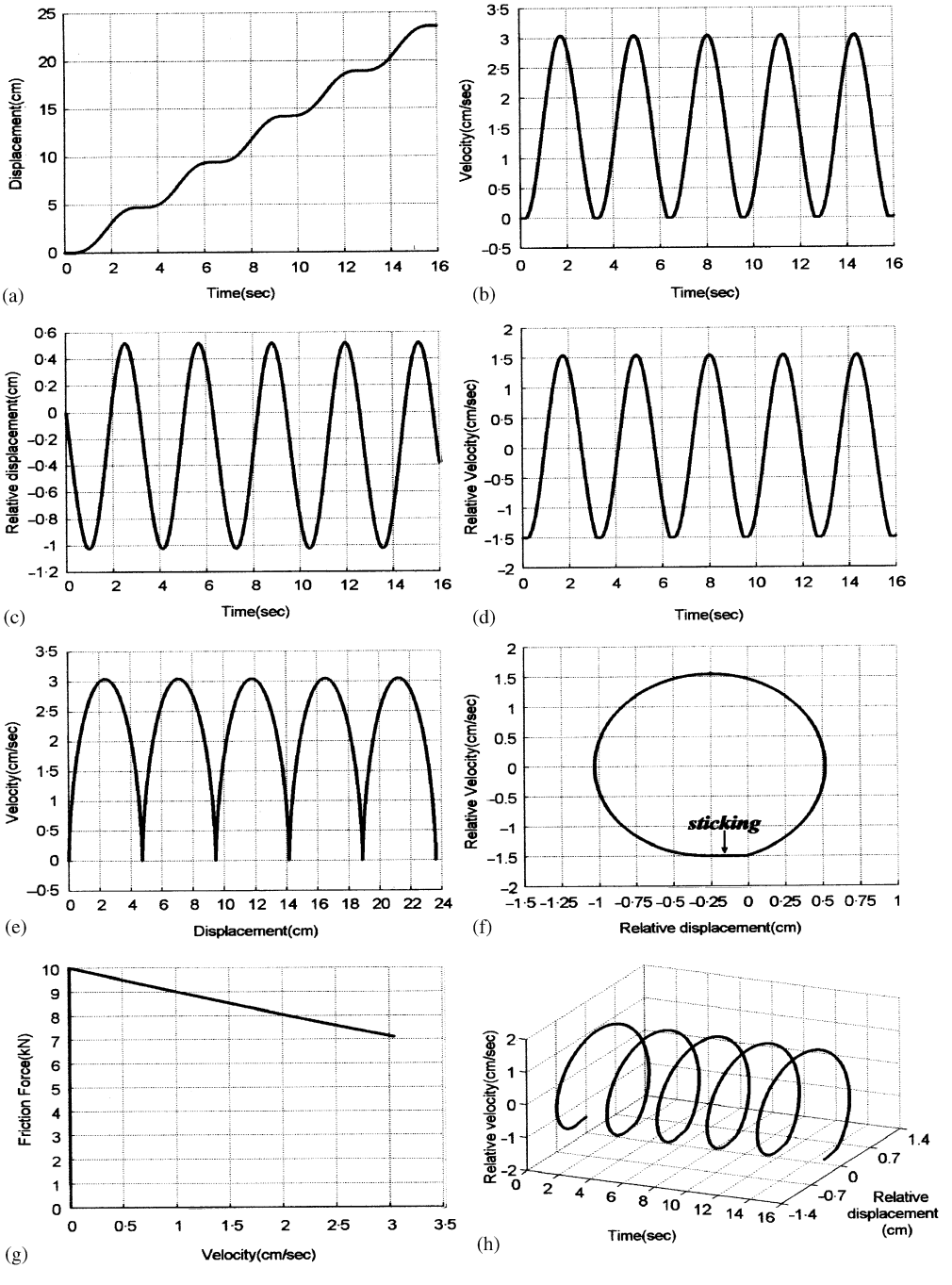

Figure 11. Time history plots and phase plots of the speed-dependent friction system with $v = 1{\cdot}5\,\text{cm/s}$.

For this case, the oscillating amplitudes of the velocity $\dot{x}$, of the relative displacement z and of its velocity $\dot{z}$ are all slowly decreased to some certain values. In the phase plane $(z, \dot{z})$, the trajectory is spiraled gradually to an ellipse with centre $(-0{\cdot}1675,\ 0)$ as shown in Figure 10(c).

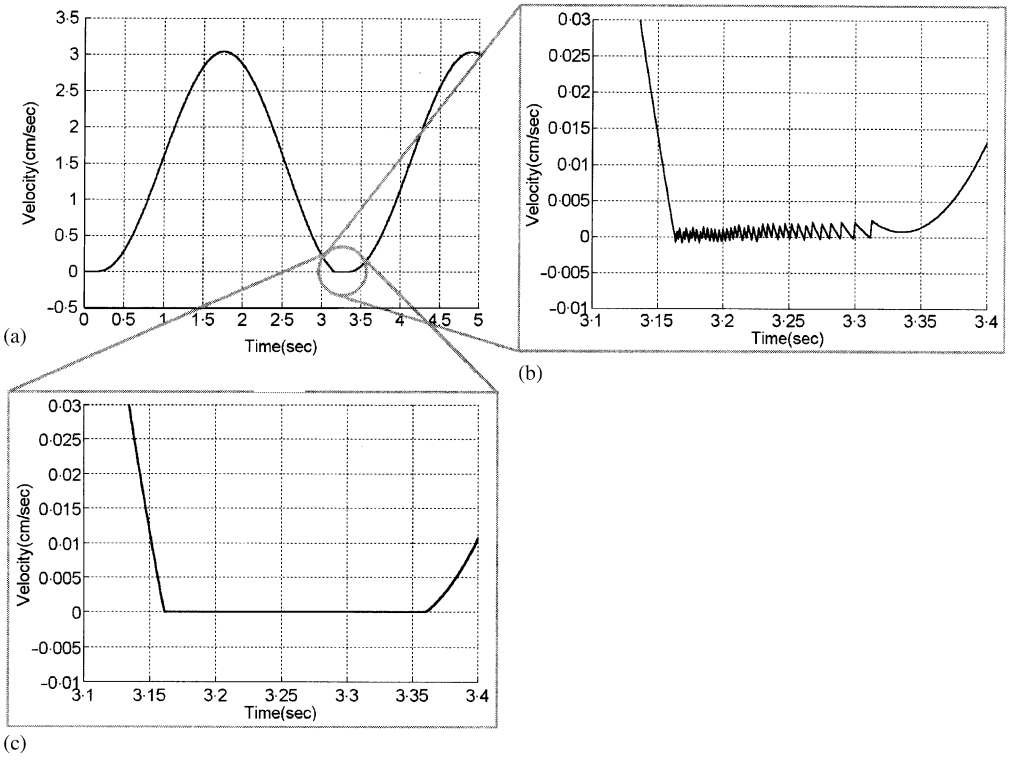

Figure 12. A refined version of the time history of the mass velocity shown in Figure 11(b).

For the last case we let the driving velocity be $v = 1{\cdot}5\,\text{cm/s}$, at which the equilibrium point becomes unstable, and instead we have a stable limit cycle as shown in Figure 11(f). This indicates that when $v > v^*$, the mass slider motion tends to a stable equilibrium point, and when $v < v^*$, the mass slider motion tends to a stable limit cycle. That is, the system undergoes a subcritical Hopf bifurcation when v varies from $v > v^*$ to $v < v^*$. From Figure 11 it can be seen that the oscillating amplitudes of the velocity $\dot{x}$, of the relative displacement z and of its velocity $\dot{z}$ are all constant. In the phase plane $(z, \dot{z})$, the trajectory is a limit cycle with a short sticking phase in the bottom. The period of the motion is about 3 s, and within each period the duration of the sticking phase is about one-half second. At the sticking phase $\dot{x} = 0$; however, by numerical solutions it is hard to match this condition. A refined version of the plot in Figure 11(b) is amplified to investigate the numerical result as shown in Figure 12. The numerical values are close to zero but exhibit an irregular burst with height among 0·002–0·0025 cm/s as shown in Figure 12(b). However, we can avoid this irregular burst by letting $|\dot{x}| < \varepsilon$ instead of $|\dot{x}| = 0$, where ε is a positive small number. In Figure 12(c) we show such a refined version with $\varepsilon = 0{\cdot}0025\,\text{cm/s}$.

From the time history plot as shown in Figure 11(a) we know that the mass slider has a climb motion. For the uniformity of the mass transmission we want to avoid such type of motion. Figure 13 displays the slide–stick motion region of the system in the parametric plane (c, v). To avoid climb motion of the mass slider, the driving velocity must be large enough so as to be $v > v^*$.

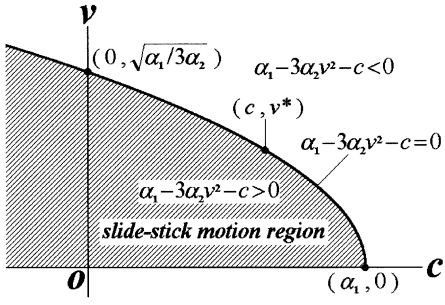

Figure 13. Slide–stick motion region in the parametric plane (c, v) for the speed-dependent friction system.

10. CONCLUSIONS

For both the belt-driven and periodically excited system we have derived closed-form solutions according to a more complete two-phase formulation, and some interesting behaviours of the considered system were displayed. For the non-damping oscillator with belt being fixed, we have provided closed-form formulae for estimating the maximum displacement and the minimum driving speed amplitude needed to prevent mass from sticking to the belt. Despite the deceiving simplicity of the model used to simulate the mass transmission behaviour by considering friction, its non-linear dynamic behaviour may represent the qualitative response of the more general transmission system. In this paper we have considered two friction laws for the mass transmission device. For the Coulomb friction system the positive damping term suffices to avoid the climb motion of the mass slider, and hence slide–stick phenomena can be avoided. For the speed-dependent friction system we have identified a critical speed v^*. According to the qualitative analysis in the phase plane, we give simple criteria of the parameter values for the stable equilibrium point as well as for the stable limit cycle. When v varies from $v > v^*$ to $v < v^*$, subcritical Hopf bifurcation occurs. For the latter case, the mass slider climbs forward, sliding is interrupted by sticking, but by increasing the driving speed the climb motion can be avoided.

REFERENCES

1. J. Den Hartog 1931 *Transaction of the American Society of Mechanical Engineers* **53**, 107–115. Forced vibrations with combined Coulomb and viscous friction.
2. M. S. Hundal 1979 *Journal of Sound and Vibration* **64**, 371–378. Response of a base excited system with Coulomb and viscous friction.
3. N. Makris and M. C. Constantinou 1991 *Mechanics of Structure and Machine* **19**, 477–500. Analysis of motion resisted by friction. I. Constant Coulomb and linear Coulomb friction.
4. H.-K. Hong and C.-S. Liu 2000 *Journal of Sound and Vibration* **229**, 1171–1192. Coulomb friction oscillator: modelling and responses to harmonic loads and base excitations.
5. H.-K. Hong and C.-S. Liu 2001 *Journal of Sound and Vibration* **244**, 883–898. Non-sticking oscillation formulae for Coulomb friction under harmonic loading.
6. C.-S. Liu 2001 *Journal of Marine Science and Technology* **9**, 122–129. Coulomb friction applied to analyze the cutting vibration of tool on workpiece.
7. K. Popp, N. Hinrichs and M. Oestreich 1996 in *Dynamics with Friction* (A. Guran, F. Pfeiffer and K. Popp, editors), 1–35. World Scientific: Singapore. Analysis of a self-excited friction oscillator with external excitation.
8. U. Andreaus and P. Casini 2001 *Journal of Sound and Vibration* **245**, 685–699. Dynamics of friction oscillators excited by a moving base and/or driving force.

9. J. R. Alifov and K. V. Frolov 1979 *Mekhanika Tverdogo Tela* **14**, 25–33. Investigation of self-excited oscillations with friction under conditions of parametric excitation and limited power of energy source.
10. A. Tondol 1992 *Quenching of Self-excited Vibrations*. Elsevier: New York.
11. J. L. Moiola and G. Chen 1996 *Hopf Bifurcation Analysis: a Frequency Domain Approach*. World Scientific: Singapore.
12. C.-S. Liu 2000 *International Journal of Non-Linear Mechanics* **35**, 931–946. Intermittent transition to quasiperiodicity demonstrated via a circular differential equation.
13. C.-S. Liu 2001 *International Journal of Non-Linear Mechanics* **36**, 1047–1068. Cone of non-linear dynamical system and group preserving schemes.